# Goldstone Solar System Radar Signal Processing

R. Jurgens, E. Satorius, and O. Sanchez
Communications Systems Research Section

*A performance analysis of the planetary radar data acquisition system is presented. These results extend previous computer simulation analysis and are facilitated by the development of a simple analytical model that predicts radar system performance over a wide range of operational parameters. The results of this study are useful to both the radar systems designer and the science investigator in establishing operational radar data acquisition parameters which result in the best systems performance for a given set of input conditions.*

## I. Introduction

In a previous article [1], a system performance analysis of the Goldstone Solar System Radar (GSSR) high-speed data acquisition system was presented. For range-Doppler mapping applications, the system uses a binary phase-coded (BPC) transmitted waveform and the received echoes are complex basebanded, sampled, and demodulated with a replica of the transmitted BPC waveform. The system comprises high-speed digital front-end filters and complex demodulators as well as operator monitor and control, data recording, and real-time signal processing (in a general-purpose, VAX 11/780 host computer equipped with an FPS-5210 array processor). The real-time signal processing activities include the generation of range-Doppler maps.

The analysis in [1] was based on a computer simulation model of the digital baseband data paths. In this article, the previous results are extended with the development of a simple analytical model for the digital baseband data paths. This analytical model is based on a quantized Gaussian approximation for the digitized inputs to the baseband demodulators (correlators/accumulators) and predicts the system processing gain as a function of the various input and operational parameters. The result provides a characterization of system performance that is useful to both the radar system designer as well as the planetary radar science investigator.

In Section II of this article, an overview of the GSSR data acquisition ranging system and its theoretical (ideal) performance is provided, and in Section III the analytical model for the digital baseband data paths is presented. Then, in Section IV, predicted performance analysis results obtained with this model are presented and compared with the results obtained from the computer simulation model. Generally there is good agreement except for those parameter regions where the analytical model is not valid, e.g., in regions where signal clipping distortion occurs at the front-end A/D converters.

## II. System Overview

Prior to developing the analytical model for the GSSR data acquisition system, a brief overview of the system architecture as well as a comprehensive review of its theoretical (ideal) performance in terms of the processing gain is presented.

## A. System Architecture

As noted in [1], the GSSR data ranging system comprises multiple, complex baseband data channels. The block diagram for a single complex data path is presented in Fig. 1. In this article as in [1], the focus is on just one channel, which would correspond to monostatic, single polarization data collections.

Although limited to a single channel, the results presented here can be used to understand trends in multichannel system performance as a function of the various input system parameters.

To summarize from [1], both in-phase and quadrature channels are low-pass filtered (LPF) (to 6 MHz) and sampled (nominally at 40 MHz). The sampled data streams are then input to pre- and postbaud integrating filters. The prebaud filter integrates five input samples per output data sample and the postbaud filter integrates $N_{BAUD}$ input samples per output data sample ($N_{BAUD}$ is user specified).

The data paths out of the A/D converters are 8 bits wide, but are expanded to 16 bits after the prebaud integrators. A further expansion to 32 bits occurs after multiplication by the scaling constant so that the postbaud integration is carried out with 32-bit integer arithmetic. Following postbaud integration, the data are truncated to $N_{BITS}$ ($N_{BITS}$ is nominally 4) and are then correlated and accumulated to produce a stream of correlation data that are output to the system computer.

## B. Ideal System Performance Analysis

To facilitate the presentation of the statistical performance model in Section III and to provide a point of comparison, a comprehensive review is presented here of the ideal (i.e., in the absence of A/D nonlinearities or digitization errors) processing gain for the GSSR data acquisition system. The basic function of the system (prior to the host computer) is to correlate contiguous segments of the received echoes with a replica of the transmitted BPC waveform:

$$\phi_i(\tau) = \int_{iT}^{(i+1)T} dt\; x(t)\; BPC(t+\tau) \qquad (1)$$

where $x(t)$ is the received complex basebanded data (just prior to the A/D converters) and $BPC(t)$ denotes the BPC waveform which is a periodic binary-valued ($BPC = \pm 1$), pseudo-noise (PN) sequence generated by a linear shift register [2]. $T$ is the period of the BPC waveform:

$$T = \Delta T\; N_{CODE}$$

where $N_{CODE}$ denotes the pseudo-noise (PN) code period and $\Delta T$ denotes the duration of a single code element (baud).

In carrying out the ideal system performance analysis, it is assumed that the input A/D converters perform only time sampling without amplitude quantization, i.e., the assumption of infinite A/D numerical precision. In this case, the time-sampled (complex) output from the A/D converters is represented simply by

$$x(k) \equiv x\,(kT_s)$$

where $F_s \equiv 1/T_s$ denotes the AD input sampling rate.

With reference to Fig. 1 but assuming that all operations depicted in Fig. 1 are performed with infinite numerical precision,[1] the sampled complex data, $x(k)$, are easily traced through the system. Specifically, at the output of the prebaud integrators (which are typically subsampled by a factor of 5),

$$x_{PRE}(k) = \sum_{n=0}^{4} x(5k-n) \qquad (2)$$

and at the output of the postbaud integrators (which are typically subsampled by a factor of $N_{BAUD}$),

$$x_{POST}(k) = \sum_{n=0}^{N_{BAUD}-1} x_{PRE}\,(N_{BAUD}k - n)$$

$$= \sum_{n=0}^{5N_{BAUD}-1} x\,(5N_{BAUD}k - n) \qquad (3)$$

Note that the sample rate out of the postbaud integrators is reduced by the factor $5N_{BAUD}$ from the input A/D sample rate, $F_s$.

Given the discrete-time representation of the complex data from Eq. 3, the correlation function (Eq. (1)) can be written in discretized form as:

[1] In the following, ignore all the operations in Fig. 1 that are connected with finite numerical precision implementation effects, i.e., the scaling multiplication and bit truncation operations.

$$c(i,k) \equiv \phi_i(k\Delta T)$$

$$= \sum_{n=iN_T}^{(i+1)N_T-1} x_{POST}(n) BPC\{5N_{BAUD}T_s n + k\Delta T\} \quad (4)$$

where $N_T$ denotes the number of (decimated) time samples out of the postbaud integrator per PN code period, $T$. Given that the time interval between samples of $x_{POST}(k)$ is $5N_{BAUD}T_s$ (Eq. (3)), $N_T$ is given by $N_T = T/(5N_{BAUD}T_s)$.

In Eq. (4), the authors tacitly assume that successive samples of the correlation function, $c(i,k-1)$ and $c(i,k)$, are separated in time by a code baud element, $\Delta T$. In practice, this time separation can be a fraction of $\Delta T$ simply by controlling $N_{BAUD}$.

Prior to developing the ideal system performance analysis, a model for the input data, $x(t)$ was acquired. Here the authors assume that the received complex basebanded data are comprised of the received signal and additive noise:

$$x(k) = s(k) + n(k) \quad (5)$$

where $s(k)$ is modeled as a Doppler-shifted and scaled version of the transmitted BPC waveform:

$$s(k) = A\ BPC(kT_s)\, e^{j\theta} e^{2\pi j k \Delta f T_s} \quad (6)$$

$A$ denotes the amplitude scaling (received amplitude level), $\theta$ is an arbitrary phase offset (assumed to be a random variable, uniformly distributed between $-\pi$ and $\pi$) and $\Delta f$ denotes the Doppler shift.

Following postbaud integration (from Eqs. (3) and (5)),

$$x_{POST}(k) = \sum_{m=0}^{5N_{BAUD}-1} x(5N_{BAUD}k - m)$$

$$= \sum_{m=0}^{5N_{BAUD}-1} s(5N_{BAUD}k - m)$$

$$+ \sum_{m=0}^{5N_{BAUD}-1} n(5N_{BAUD}k - m)$$

$$\equiv s_{POST}(k) + n_{POST}(k) \quad (7)$$

Assuming that the time interval between samples of $x_{POST}(k)$, i.e., $5N_{BAUD}T_s$, is matched to a baud interval, $\Delta T$ (or less), and that the Doppler offset is much less than $1/\Delta T$,

$$s_{POST}(k) \approx 5N_{BAUD}\ s(5N_{BAUD}k)$$

$$= 5N_{BAUD}A \cdot BPC\{5N_{BAUD}kT_s\}\, e^{j\theta} e^{2\pi j 5N_{BAUD}k\Delta f T_s} \quad (8)$$

The signal-to-noise ratio (SNR) output from the postbaud integrators is thus given by

$$SNR_{POST} = \frac{\langle |s_{POST}|^2 \rangle}{\langle |n_{POST}|^2 \rangle} = \frac{\{5N_{BAUD}A\}^2}{\langle |n_{POST}|^2 \rangle} \quad (9)$$

where $< \cdot >$ denotes statistical expectation. From Eq. (7),

$$\langle |n_{POST}|^2 \rangle = \sum_{m,m'=0}^{5N_{BAUD}-1} \langle n(5N_{BAUD}k - m)\ n^*(5N_{BAUD}k - m') \rangle \quad (10)$$

Assuming that the input low-pass filters (see Fig. 1) are ideal and thus that the input power spectrum of the additive noise (just prior to the A/D converters) is constant out to the cutoff frequency, $f_{CO}$, of the filters,

$$\langle n(5N_{BAUD}k-m)\,n^*(5N_{BAUD}k-m')\rangle = \langle|n|^2\rangle \frac{\sin\{2\pi f_{CO}T_s(m-m')\}}{2\pi f_{CO}T_s(m-m')} \tag{11}$$

Substituting Eq. (11) into Eq. (10),

$$\langle|n_{POST}|^2\rangle = \langle|n|\rangle^2 \sum_{m,m'=0}^{5N_{BAUD}-1} \frac{\sin\{2\pi f_{CO}T_s(m-m')\}}{2\pi f_{CO}T_s(m-m')}$$

$$= 5N_{BAUD}\langle|n|^2\rangle \sum_{m=-(5N_{BAUD}-1)}^{5N_{BAUD}-1} \left(1-\frac{|m|}{5N_{BAUD}}\right) \frac{\sin\{2\pi f_{CO}T_s m\}}{2\pi f_{CO}T_s m} \tag{12}$$

Provided that the low-pass filtered noise coherence is significantly shorter than the combined pre- and postbaud integration time constant, $5N_{BAUD}T_s$, this approximation can be made:

$$OS \equiv \sum_{m=-(5N_{BAUD}-1)}^{5N_{BAUD}-1} \left(1-\frac{|m|}{5N_{BAUD}}\right) \frac{\sin\{2\pi f_{CO}T_s m\}}{2\pi f_{CO}T_s m}$$

$$\approx \sum_{m=-\infty}^{\infty} \frac{\sin\{2\pi f_{CO}T_s m\}}{2\pi f_{CO}T_s m} = \frac{1}{2f_{CO}T_s} \tag{13}$$

Plots of $\{2f_{CO}T_sOS\}$ versus $f_{CO}T_s$, for different values of $L \equiv 5N_{BAUD}-1$, are presented in Fig. 2. As is seen, the approximation in Eq. (13) is accurate to within, at most, a 10-percent error over a wide range of parameter values. As a typical example, consider the nominal system parameters, $f_{CO}T_s = (6\text{ MHz})/(40\text{ MHz}) = 0.15$ and assume that the combined baud integrator time constant is matched to a 1-$\mu$sec baud BPC code element, i.e., $5N_{BAUD} = \Delta T/T_s = 1\mu\text{sec} \times 40\text{ MHz} = 40$. Then, it is seen from Fig. 2 that the approximation in Eq. (13) is accurate to within approximately 2.5 percent ($2f_{CO}T_sOS \approx 0.975$), which corresponds to a difference of only 0.1 dB between the actual noise power, $\langle|n_{POST}|^2\rangle$, and its estimate based on the approximation in Eq. (13).

The factor $OS$ is referred to as the "noise oversampling factor," which indicates the degree of dependence of the noise samples (out of the A/D). As $f_{CO}$ approaches Nyquist, $1/2T_s$, there is no oversampling, and $OS = 1$. For $f_{CO} < 1/2T_s$, $OS > 1$, indicating noise oversampling beyond the minimum Nyquist rate. Substituting Eq. (12) (with Eq. (13)) into Eq. (9) yields the following expression for SNR at the output of the postbaud integrators:

$$SNR_{POST} = \frac{\{5N_{BAUD}A\}^2}{\langle|n_{POST}|^2\rangle} \approx \frac{5N_{BAUD}A^2}{OS\langle|n|^2\rangle} \equiv \frac{5N_{BAUD}}{OS}SNR_{IN} \tag{14}$$

where $SNR_{IN}$ denotes the input SNR (referenced to the output of the ideal A/D converters).

To finally characterize the ideal system performance, the discretized correlation function (Eq. (4)) is used along with Eqs. (7) and (8):

$$c(i,k) = \sum_{m=iN_T}^{(i+1)N_T-1} x_{POST}(m)BPC\{5N_{BAUD}mT_s + k\Delta T\}$$

$$= \sum_{m=iN_T}^{(i+1)N_T-1} [5N_{BAUD}Ae^{j\theta}e^{2\pi 5N_{BAUD}m\Delta fT_s}BPC\{5N_{BAUD}mT_s\}$$

$$+n_{POST}(m)]\,BPC\{5N_{BAUD}mT_s + k\Delta T\}$$

$$\equiv S_i(k) + N_i(k) \tag{15}$$

where

$$S_i(k) = 5N_{BAUD}Ae^{j\theta}\sum_{m=iN_T}^{(i+1)N_T-1} e^{2\pi j5N_{BAUD}m\Delta fT_s}BPC\{5N_{BAUD}mT_s\}$$

$$\cdot\ BPC\{5N_{BAUD}mT_s + k\Delta T\} \tag{16a}$$

and

$$N_i(k) = \sum_{m=iN_T}^{(i+1)N_T-1} n_{POST}(m)BPC\{5N_{BAUD}mT_s + k\Delta T\} \tag{16b}$$

The system computer transforms the correlation data into range-Doppler maps, $RD(k,m)$, as follows:

$$RD(k,m) = \sum_{i=0}^{N_{BINS}-1} c(i,m)e^{-2\pi jki/N_{BINS}} \tag{17}$$

where $N_{BINS}$ denotes the number of Doppler frequency bins. The maximum value of $RD(k,m)$ occurs when $m$ is such that the local code replica is perfectly aligned with the received code and when $2\pi k/N_{BINS}$ coincides with the Doppler shift of the received signal, subsampled by $\{5N_{BAUD}N_T\}$, i.e.,

$$2\pi k/N_{BINS} = \{2\pi 5N_{BAUD}\Delta fT_s\}\,N_T \equiv \{\Delta\omega\}\,N_T$$

where $\Delta\omega$ denotes the Doppler shift of the received signal normalized by the decimated sample rate at the output of the postbaud integrators. Thus,

$$RD_{MAX} = \sum_{i=0}^{N_{BINS}-1} c(i,0)e^{-j(\Delta\omega N_T)i}$$

$$= \sum_{i=0}^{N_{BINS}-1} S_i(0)e^{-j(\Delta\omega N_T)i} + \sum_{i=0}^{N_{BINS}-1} N_i(0)e^{-j(\Delta\omega N_T)i}$$

$$\equiv S + N \tag{18}$$

By virtue of the definition of $S_i(k)$ (Eq. (16a)),

$$S = 5N_{BAUD}Ae^{j\theta}\sum_{i=0}^{N_{BINS}-1}\left\{\sum_{m=iN_T}^{(i+1)N_T-1}e^{j\Delta\omega m}\right\}e^{-j(\Delta\omega N_T)i}$$

$$= 5N_{BAUD}Ae^{j\theta}\frac{1-e^{j\Delta\omega N_T}}{1-e^{j\Delta\omega}}N_{BINS} \equiv 5N_{BAUD}Ae^{j\theta}\Psi(\Delta\omega; N_T)\,N_{BINS} \tag{19a}$$

where

$$\Psi(\Delta\omega; N_T) = \frac{1-e^{j\Delta\omega N_T}}{1-e^{j\Delta\omega}} \tag{19b}$$

The factor $\Psi(\Delta\omega; N_T)\,N_{BINS}$ represents the coherent integration time constant of the system. When $\Delta f \ll 1/T$, $\Delta\omega N_T \ll 1, \Psi(\Delta\omega; N_T) \approx N_T$, and the coherent integration time constant approaches $N_T N_{BINS}$.

To conveniently characterize the system performance, the authors define the system processing gain, which is simply the ratio of output to input SNR. The output SNR ($SNR_0$) is referenced with respect to the output range-Doppler map. Specifically,

$$SNR_0 = \frac{\langle|S|^2\rangle}{\langle|N|^2\rangle} \tag{20}$$

where (from Eq. (19))

$$\langle|S|^2\rangle = \{5AN_{BAUD}N_{BINS}\}^2\{\sin(\Delta\omega N_T/2)/\sin(\Delta\omega/2)\}^2 \tag{21}$$

and (from Eq. (18)),

$$\langle|N|^2\rangle = \sum_{i,i'=0}^{N_{BINS}-1}\langle N_i(0)N_i^*,(0)\rangle = \sum_{i-0}^{N_{BINS}-1}\langle|N_i(0)|^2\rangle \tag{22}$$

The last equality in Eq. (22) follows from the independence of the noise samples, $N_i(k)$. From Eq. (16b),

$$\langle|N_i(0)|^2\rangle = \sum_{m,m'=iN_T}^{(i+1)N_T-1}BPC\{5N_{BAUD}mT_s\}\,BPC\{5N_{BAUD}m'T_s\}$$

$$\cdot\langle n_{POST}(m)n_{POST}^*(m')\rangle \tag{23}$$

But recall that the coherence of the input noise is sufficiently short that samples of $n_{POST}(m)$ are independent (i.e., the assumption leading to Eq. (13)). Thus, from Eqs. (12), (13), (22), and (23),

$$\langle |N|^2 \rangle = \sum_{i=0}^{N_{BINS}} \langle |N_i(0)|^2 \rangle = \sum_{i=0}^{N_{BINS}-1} \sum_{m=iN_T}^{(i+1)N_T-1} \langle |n_{POST}(m)|^2 \rangle$$

$$= \langle |n|^2 \rangle 5N_{BAUD}OSN_TN_{BINS} \tag{24}$$

and therefore, from Eqs. (21) and (24),

$$SNR_0 = \frac{\{5AN_{BAUD}N_{BINS}\}^2 \{\sin(\Delta\omega N_T/2)/\sin(\Delta\omega/2)\}^2}{\langle |n|^2 \rangle 5N_{BAUD}OSN_TN_{BINS}}$$

$$= \frac{1}{OS}5N_{BAUD}N_{BINS}\left[\frac{\{\sin(\Delta\omega N_T/2)\}^2}{N_T\{\sin(\Delta\omega/2)\}^2}\right] SNR_{IN} \tag{25}$$

Thus, for the ideal system performance gain,

$$PG_{IDEAL} \equiv \frac{SNR_0}{SNR_{IN}} = \frac{1}{OS}5N_{BAUD}N_{BINS}\left[\frac{\{\sin(\Delta\omega N_T/2)\}^2}{N_T\{\sin(\Delta\omega/2)\}^2}\right] \tag{26}$$

As $\Delta\omega$ approaches zero, $PG_{IDEAL}$ can be expressed in terms of the system time-bandwidth product, i.e., from Eq. (13),

$$PG_{IDEAL}(\Delta\omega = 0) = 2f_{CO}T_s\ 5N_{BAUD}N_{BINS}N_T \equiv 2f_{CO}T_{COH} \tag{27}$$

where $T_{COH}$ denotes the total coherent processing time and $(2f_{CO})$ is the system bandwidth. This agrees with the result presented in [1].

## III. Statistical System Performance Model

Having provided a general basis for understanding ideal system performance, here is a simple, approximate performance analysis that takes into account finite numerical precision effects. Specifically, with reference to Fig. 1, it is seen that two sources of amplitude quantization errors arise: (1) at the A/D converters and (2) following the postbaud integrators. In the authors' simplified approximate analysis, the A/D amplitude quantization is ignored,[2] but the quantization after the postbaud integrators (at the input to the correlators) is taken into account. Thus, the quantized correlator outputs can be expressed in complex form, as follows:

$$c_Q(i,k) = \sum_{m=iN_T}^{(i+1)N_T-1} Q\left[A'e^{j(\Delta\omega m+\theta)}BPC\{\alpha m\} + n_{POST}(m)\right] BPC\{\alpha m + k\Delta T\} \tag{28}$$

where again $\Delta\omega \equiv 2\pi 5N_{BAUD}\Delta f T_s$, $A' \equiv 5AN_{BAUD}$, $\alpha = 5N_{BAUD}T_s$, and $Q[\cdot]$ denotes the nonlinear quantizer with $Q[x+jy] \equiv Q[x] + jQ[y]$ operation. In the following, it is assumed that $Q(x) = -Q(-x)$.

[2] This is reasonable since the A/D converters are nominally 8 bits wide (compared to nominally 4 bits at the correlator inputs) and the outputs from the A/D converters are smoothed by the pre- and postbaud integrators. Thus, the effects of A/D quantization on system performance (processing gain) are typically much less important than the effects of input correlator quantization.

As discussed in Section II (Eqs. (17) through (20)), system performance can be characterized in terms of the maximum range-Doppler map output, $RD_{MAX}$. For the case of quantized input correlator data,

$$RD_{MAX} = \sum_{i=0}^{N_{BINS}-1} c_Q(i,0)e^{-j(\Delta\omega N_T)i} \tag{29}$$

and the output SNR is defined as

$$SNR_0 = \frac{\langle |RD_{MAX}|^2 \rangle - \langle |RD_{MAX}|^2_{A'=0} \rangle}{\langle |RD_{MAX}|^2_{A'=0} \rangle} \tag{30}$$

where the subscript $A' = 0$ is used to denote the noise-only input condition.

Maximum map output, $\langle |RD_{MAX}|^2 \rangle$, can be expressed in terms of the statistics of the quantized correlator outputs, $c_Q(i,0)$:

$$\langle |RD_{MAX}|^2 \rangle = \sum_{i=0}^{N_{BINS}-1} \sum_{i'=0}^{N_{BINS}-1} \langle c_Q(i,0)c_Q^*(i',0) \rangle e^{-j(\Delta\omega N_T)(i-i')} \tag{31}$$

To proceed, the notation is simplified by expressing $c_Q(i,0)$ as

$$c_Q(i,0) = \sum_{m=iN_T}^{(i+1)N_T-1} \{Q[x_R(m)] + jQ[x_I(m)]\} BPC\{\alpha m\} \tag{32}$$

where

$$x_R(m) = A' \cos[\Delta\omega m + \theta] BPC(\alpha m) + Re\{n_{POST}(m)\} \tag{33a}$$

and

$$x_I(m) = A' \sin[\Delta\omega m + \theta] BPC(\alpha m) + Im\{n_{POST}(m)\} \tag{33b}$$

Assuming that $Re\{n_{POST}(m)\}$ and $Im\{n_{POST}(m)\}$ are uncorrelated zero-mean Gaussian noise components with

$$\left\langle [Re\{n_{POST}\}]^2 \right\rangle = \left\langle [Im\{n_{POST}\}]^2 \right\rangle \equiv \sigma^2$$

then note that $x_R$ and $x_I$ are independent random variables with conditional Gaussian densities:

$$p_R(x_R|\theta) = \frac{1}{\sqrt{2\pi\sigma^2}} \exp\left\{ -[x_R - A' \cos(\Delta\omega m + \theta) BPC(\alpha m)]^2 / 2\sigma^2 \right\} \tag{34a}$$

and

$$p_I(x_I|\theta) = \frac{1}{\sqrt{2\pi\sigma^2}} \exp\left\{-\left[x_I - A' \sin(\Delta\omega m + \theta)\, BPC(\alpha m)\right]^2 / 2\sigma^2\right\} \tag{34b}$$

In the subsequent development, the following moment functions, based on $p_R$ and $p_I$, will be used:

$$\Phi_1(x) = \frac{1}{\sqrt{2\pi\sigma^2}} \int_{-\infty}^{\infty} Q(u) \exp\left\{-[u-x]^2 / 2\sigma^2\right\} du \tag{35a}$$

and

$$\Phi_2(x) = \frac{1}{\sqrt{2\pi\sigma^2}} \int_{-\infty}^{\infty} \{Q(u)\}^2 \exp\left\{-[u-x]^2 / 2\sigma^2\right\} du \tag{35b}$$

By virtue of the odd property of $Q(u)$, it is easy to see that $\Phi_1(x)$ is also odd (with $\Phi_1(0) = 0$) and $\Phi_2(x)$ is even.

Now consider the evaluation of $SNR_0$. Specifically, from Eq. (32),

$$\begin{aligned}\left\langle c_Q(i,0) c_Q^*(i',0)\right\rangle = \sum_{m=iN_T}^{(i+1)N_T-1} \sum_{m'=i'N_T}^{(i'+1)N_T-1} \{&[\langle Q(x_R(m))\, Q(x_R(m'))\rangle \\ &+ \langle Q(x_I(m))\, Q(x_I(m'))\rangle] \\ &+ j\left[\langle Q(x_I(m))\, Q(x_R(m'))\rangle - \langle Q(x_R(m))\, Q(x_I(m'))\rangle\right]\} BPC(\alpha m) BPC(\alpha m')\end{aligned} \tag{36}$$

In evaluating Eq. (36), two cases are distinguished: $i = i'$ and $i \neq i'$. In the latter case, all terms in the expectations are conditionally independent (with respect to $\theta$) and with Eq. (35),

$$\begin{aligned}\left\langle c_Q(i,0) c_Q^*(i',0)\right\rangle = \sum_{m=iN_T}^{(i+1)N_T-1} \sum_{m'=i'N_T}^{(i'+1)N_T-1} \{&[\langle \Phi_1(A' \cos(\Delta\omega m + \theta) BPC(\alpha m)) \\ &\cdot \Phi_1(A' \cos(\Delta\omega m' + \theta) BPC(\alpha m'))\rangle_\theta \\ &+ \langle \Phi_1(A' \sin(\Delta\omega m + \theta) BPC(\alpha m)) \Phi_1(A' \sin(\Delta\omega m' + \theta) BPC(\alpha m'))\rangle_\theta] \\ &+ j\left[\langle \Phi_1(A' \sin(\Delta\omega m + \theta) BPC(\alpha m))\, \Phi_1(A' \cos(\Delta\omega m' + \theta) BPC(\alpha m'))\rangle_\theta\right. \\ &\left. - \langle \Phi_1(A' \cos(\Delta\omega m + \theta) BPC(\alpha m)) \Phi_1(A' \sin(\Delta\omega m' + \theta) BPC(\alpha m'))\rangle_\theta]\right\} \\ &\cdot BPC(\alpha m) \cdot BPC(\alpha m'), \text{ for } i \neq i'\end{aligned} \tag{37}$$

where

$$\langle f(\theta)\rangle_\theta \equiv \frac{1}{2\pi}\int_{-\pi}^{\pi} f(\theta)d\theta \tag{38}$$

By virtue of the oddness of $\Phi_1(x)$ (and recalling that $BPC = \pm 1$),

$$\Phi_1(xBPC(\alpha m))BPC(\alpha m) = \Phi_1(x), \text{ for any } x$$

Thus, from Eq. (37) and for $i \neq i'$,

$$\begin{aligned}\langle c_Q(i,0)c_Q(i',0)\rangle = \sum_{m=iN_T}^{(i+1)N_T-1}\sum_{m'=iN_T}^{(i'+1)N_T-1} \{[\langle\Phi_1(A'\cos(\Delta\omega m + \theta))\Phi_1(A'\cos(\Delta\omega m' + \theta))\rangle_\theta \\ + \langle\Phi_1(A'\sin(\Delta\omega m + \theta))\Phi_1(A'\sin(\Delta\omega m' + \theta))\rangle_\theta] \\ + j[\langle\Phi_1(A'\sin(\Delta\omega m + \theta))\Phi_1(A'\cos(\Delta\omega m' + \theta))\rangle_\theta \\ - \langle\Phi_1(A'\cos(\Delta\omega m + \theta))\Phi_1(A'\sin(\Delta\omega m' + \theta))\rangle_\theta]\} \\ \equiv \Gamma(i,i')\end{aligned} \tag{39}$$

When $i = i'$, the sum over $m$ and $m'$ in Eq. (36) is split into two parts: $m = m'$ and $m \neq m'$. The result for $\langle|c_Q(i,0)|^2\rangle$ is given by

$$\langle|c_Q(i,0)|^2\rangle = 2N_T\left(\langle\Phi_2(A'\cos\theta)\rangle_\theta - \langle\{\Phi_1(A'\cos\theta)\}^2\rangle_\theta\right) + \Gamma(i,i) \tag{40}$$

where the property if $f(\theta)$ is periodic in $2\pi$, then $\langle f(\theta + x)\rangle_\theta = \langle f(\theta)\rangle_\theta$ for any $x$ is exploited. From Eqs. (30), (31), (39), and (40),

$$SNR_0 = \frac{K}{2N_T N_{BINS}\ \Phi_2(0)} \tag{41a}$$

where

$$K = 2N_T N_{BINS}\left\{\langle\Phi_2(A'\cos\theta)\rangle_\theta - \Phi_2(0) - \langle\{\Phi_1(A'\cos\theta)\}^2\rangle_\theta\right\} + \sum_{i,i'}\Gamma(i,i')e^{-j(\Delta\omega N_T)(i-i')} \tag{41b}$$

Prior to presenting plots of $SNR_0$ in the next section, first consider some limiting cases. In particular, note that as $\Delta\omega$ approaches zero, $SNR_0$ reduces to

$$SNR_0(\Delta\omega = 0) = \{\langle\Phi_2(A'\cos\theta)\rangle_\theta/\Phi_2(0)\} - 1 + \left[\langle\{\Phi_1(A'\cos\theta)\}^2\rangle_\theta/\Phi_2(0)\right]\{N_T N_{BINS} - 1\} \tag{42}$$

As a consistency check, observe that in the limit of no quantization, i.e., $Q(u) = u$, Eq. (42) reduces back to Eq. (25) for the ideal case. Specifically, when $Q(u) = u$,

$$\Phi_1\{x|Q(u) = u\} = x \quad \text{and} \quad \Phi_2\{x|Q(u) = u\} = x^2 + \sigma^2$$

in which case Eq. (42) becomes

$$SNR_0\{\Delta\omega = 0|Q(u) = u\} = \left\{\left\langle A'^2 \cos^2\theta\right\rangle_\theta / \sigma^2\right\} N_T N_{BINS} = \left\{A'^2/2\sigma^2\right\} N_T N_{BINS} \tag{43}$$

Substituting

$$A' = 5N_{BAUD}A;\ \sigma^2 = \left\langle |n_{POST}|^2\right\rangle/2 = (5/2)N_{BAUD}OS\left\langle |n|^2\right\rangle \quad \text{and} \quad SNR_{IN} = A^2/\left\langle |n|^2\right\rangle$$

reveals that Eqs. (43) and (25) (with $\Delta\omega = 0$) are indeed equivalent.

Another interesting limit is that of 1-bit quantization, i.e.,

$$Q(u) = 0.5, u \geq 0 \quad \text{and} \quad Q(u) = -0.5, u < 0 \tag{44}$$

$$\Phi_2(x) = 0.25 \quad \text{(1-bit quantization)} \tag{45}$$

and thus from Eq. (42) (assuming $\Delta\omega = 0$):

$$SNR_0\{\Delta\omega = 0|\text{1-bit quantization}\} = 4\left\langle\left\{\Phi_1(A'\cos\theta)\right\}^2\right\rangle_\theta \{N_T N_{BINS} - 1\}$$

$$\approx 4N_T N_{BINS}\left\langle\left\{\Phi_1(A'\cos\theta)\right\}^2\right\rangle_\theta \tag{46}$$

In the small signal amplitude limit,

$$\Phi_1(A'\ \cos\ \theta) = \frac{1}{\sqrt{2\pi\sigma^2}} \int_0^{A'\cos\theta} e^{-u^2/2\sigma^2} du \approx \frac{A'\ \cos\ \theta}{\sqrt{2\pi\sigma^2}} \quad \text{(1-bit quantization)} \tag{47}$$

and thus Eq. (46) reduces to

$$SNR_0\{\Delta\omega = 0|\text{1-bit quantization}\} \approx 4N_T N_{BINS}\left\langle\left\{\Phi_1(A'\cos\theta)\right\}^2\right\rangle_\theta$$

$$\approx N_T N_{BINS}(2/\pi)\left\{A'^2/2\sigma^2\right\}$$

$$= N_T N_{BINS}(2/\pi)\left\{5N_{BAUD}/OS\right\} SNR_{IN} \tag{48}$$

(small signal amplitude limit)

Comparing Eqs. (48) and (25) (with $\Delta\omega = 0$), it is seen that 1-bit quantization provides a degradation in the small signal processing gain of $10 \log_{10}(2/\pi) \approx -2$ dB over ideal performance. As will be seen in the next section, system processing gain readily approaches ideal performance as the number of bits is increased.

## IV. System Processing Gain Evaluation

In evaluating system performance, the system performance gain (defined by Eq. (26) but with $SNR_0$ computed from Eq. (41)) has been computed as a function of the various system parameters. In carrying out these calculations, assume an $L = 2^B$ level quantizer ($B$ = number of bits) defined as follows:

$$Q(u) = INT\{u\} + 0.5,\ L/2 > u \geq 0;\ \ Q(u) = L/2 - 0.5,\ u \geq L/2;\ \text{ and }\ Q(u) = -Q(-u),\ u < 0$$

where $INT\{x\}$ denotes the integer part of $x$. An illustrative example of the system performance calculations is presented in Fig. 3 where plots of performance gain (from Eqs. (26) and (41)) versus $SNR_{IN}$ are presented for various baud durations, $\Delta T$, and for both $B$ = 4-bit and 8-bit quantization. For all plots presented in Fig. 3,

$$(1/T_s) = 40 \text{ MHz};\ \ f_{CO} = 6 \text{ MHz};\ N_{BINS} = 64;\ 5N_{BAUD} = \Delta T/T_s;\ \ \Delta f = 0 \text{ Hz}$$

and the PN code period, $N_T$, is varied such that

$$PG_{IDEAL} = 2f_{CO}T_s 5N_{BAUD}\ N_{BINS}\ N_T \approx 8.2 \times 10^5 \text{ (59 dB)}$$

First, one notes in Fig. 3 the dependence of processing gain on the baud duration—especially for the 4-bit quantization cases and in the low $SNR_{IN}$ regime. Short baud intervals require less postbaud integration (smaller values of $N_{BAUD}$) resulting in a large input noise fluctuation to the correlator quantizer. Larger noise fluctuation, however, populates a greater number of quantizer levels, thereby approaching the ideal processing gain. Vice versa, longer baud intervals require more integration in the postbaud filter so that the input noise fluctuation to the correlator quantizer is reduced. Fewer quantizer levels are populated and thus the processing gain approaches the 1-bit quantizer limit:

$$PG_{1-BIT} \approx PG_{IDEAL} - 2\text{dB} \approx 57 \text{ dB}$$

Another consequence of long postbaud integration is seen in the high $SNR_{IN}$ region of the curves in Fig. 3. As $SNR_{IN}$ is increased, especially for the longer baud intervals, the input samples to the correlators will saturate the quantizers. When this occurs, $SNR_0$ will not increase with increasing $SNR_{IN}$, thereby degrading the system processing gain. For shorter baud intervals, the magnitude of the input samples to the correlators are smaller for a given $SNR_{IN}$, and thus saturation will not occur except at the highest input signal levels.

Figure 4 presents plots of performance gain (again from Eqs. (26) and (41)) versus input noise level for various baud durations, $\Delta T$, and for both $B$ = 4-bit and 8-bit quantization. For all plots presented in Fig. 4,

$$SNR_{IN} = 10^{-3};\ (1/T_s) = 40 \text{ MHz};\ f_{CO} = 6 \text{ MHz};\ N_{BINS} = 256;\ 5N_{BAUD} = \Delta T/T_s;\ \Delta f = 0 \text{ Hz}$$

and the PN code period, $N_T$, is varied so that

$$PG_{IDEAL} = 2f_{CO}T_s 5N_{BAUD} N_{BINS} N_T \approx 3.1 \times 10^6 (64.9 \text{ dB})$$

Figure 4 shows that the smallest baud intervals ($\Delta T = 0.5$ $\mu$sec) achieve ideal performance sooner (at lower input noise levels) but also result in quantizer saturation sooner—as evidenced by the decrease in system processing gain at the higher noise levels. Vice versa, as the input noise level decreases, system processing gain at both 4-bit and 8-bit quantization reduces back to the 1-bit limit. In any case, from Fig. 4 it may be concluded that ideal system performance can be achieved only over a narrower range of input noise levels when 4-bit quantization is used versus 8-bit.

To further understand system performance, Fig. 5 presents plots of the average noise-only output power, $P_{no}$ (derived from Eq. (40)):

$$P_{no} \equiv N_{BINS} \left\langle |c_Q(i,0)|^2_{A'=0} \right\rangle = 2N_T N_{BINS} \Phi_2(0) \tag{49}$$

versus the input noise level corresponding to both 4- and 8-bit correlator quantization. The other system parameters used in Fig. 5 are

$$(1/T_s) = 40 \text{ MHz};\ f_{CO} = 6 \text{ MHz};\ N_T = 255 \text{ and } 2047 \text{ (span of correlators)};\ N_{BINS} = 256; \text{ and}$$

$$5N_{BAUD} = 160(N_T = 255) \text{ and } 20(N_T = 2047)$$

Note that at low input noise levels, $P_{no}$ approaches the 1-bit limit (from Eq. (45)):

$$P_{no} \{\text{1-bit quantization}\} = 0.5 N_T N_{BINS} \approx 45 \text{ dB } (N_T = 255) \text{ or } 54 \text{ dB } (N_T = 2047)$$

As the input noise level increases, more quantizer bits are toggled and $P_{no}$ begins to increase linearly until quantizer saturation occurs. Since the onset of bit toggling occurs at lower input noise levels for 8-bit quantizers, note that the linear region is much broader for the 8-bit plots in Fig. 5. This is consistent with the superior performance of 8-bit correlator quantization as observed in Figs. 3 and 4.

Finally, in Fig. 6, model calculations of $P_{no}$ (Eq. (49)) are compared with the results of computer simulations that utilize the testbed developed in [1]. This simulator models the digital high-speed data acquisition system as depicted in Fig. 1.[3] In Fig. 6 again, plots are presented of $P_{no}$ versus the input noise level for both 4- and 8-bit correlator quantization; these plots correspond to the system parameter values

$$(1/T_s) = 40 \text{ MHz};\ f_{CO} = 6 \text{ MHz}; N_T = 255 \text{ (span of correlators)};\ N_{BINS} = 256; \text{ and } 5N_{BAUD} = 160$$

Note that as the input noise level increases, simulated performance diverges significantly from the model calculations, implying even more performance degradation at the higher input levels than would be predicted from the statistical model. This added degradation results from saturation of the input 8-bit A/D converters, which were not included in the statistical performance model. Thus, the model will provide, in general, only optimistic bounds on system performance.

## V. Conclusions

This article has characterized the performance of the planetary radar data acquisition system in terms of its processing gain. It has provided performance bounds based on both the ideal implementation (no quantization) as well as an

[3] The computer simulation program, written in Fortran 77, was originally developed to run on the Radar 331 VAX 11/780 computer (without utilizing the FPS 5210 array processor). However, in generating the results presented here, the simulation software was ported over to the JPL Cray computer (originally the X-MP and now the Y-MP). In conducting the simulations presented here the authors observe that the run times for the Cray are at least 10 to 20 times faster than the corresponding 11/780 run times.

approximate statistical model that takes into account quantization at the correlator inputs. Basically, it is found that system performance is accurately characterized by the 1-bit correlator quantizer model at low input levels and for longer code baud element intervals, $\Delta T$. As the input level increases and/or $\Delta T$ decreases, performance improves toward the ideal limit until quantizer saturation occurs (both the correlator quantizer as well as the input A/D converters). At this point, system performance varies rapidly as a function of the input level, from anywhere between the ideal limit to well below the 1-bit limit.

The results of this study are useful to both the radar systems designer as well as the science investigator in establishing operational radar data acquisition parameters which result in the best systems performance for a given set of input conditions.

## References


[1] E. Satorius and S. Brokl, "Goldstone Solar System Radar Performance Analysis," *TDA Progress Report 42-93*, vol. January–March 1988, Jet Propulsion Laboratory, Pasadena, California, pp. 302–308, May 15, 1988.

[2] F. MacWilliams and N. Sloan, "Pseudo-Random Sequences and Arrays," *Proc. IEEE*, vol. 64, pp. 1715–1729, 1976.

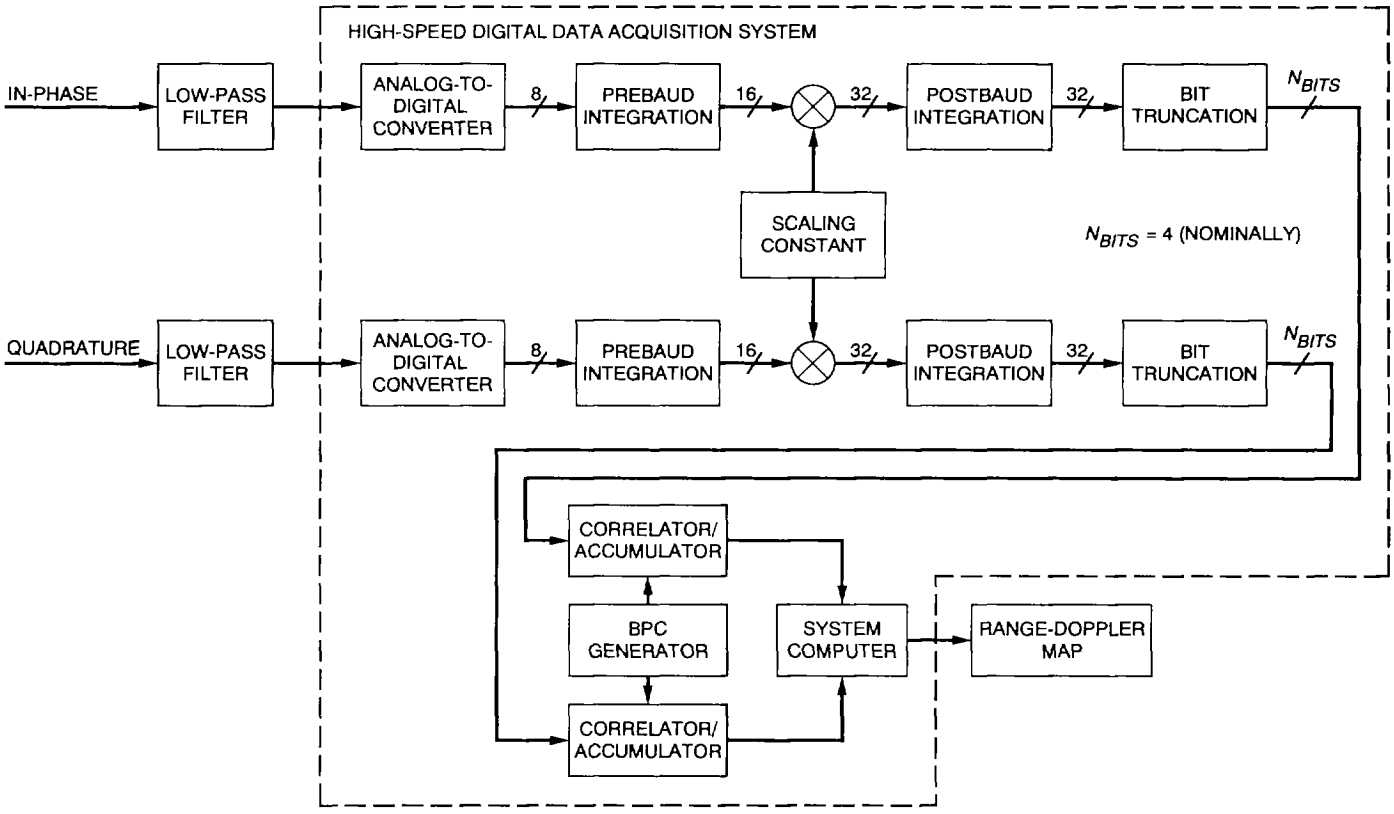


**Fig. 1. System block diagram.**

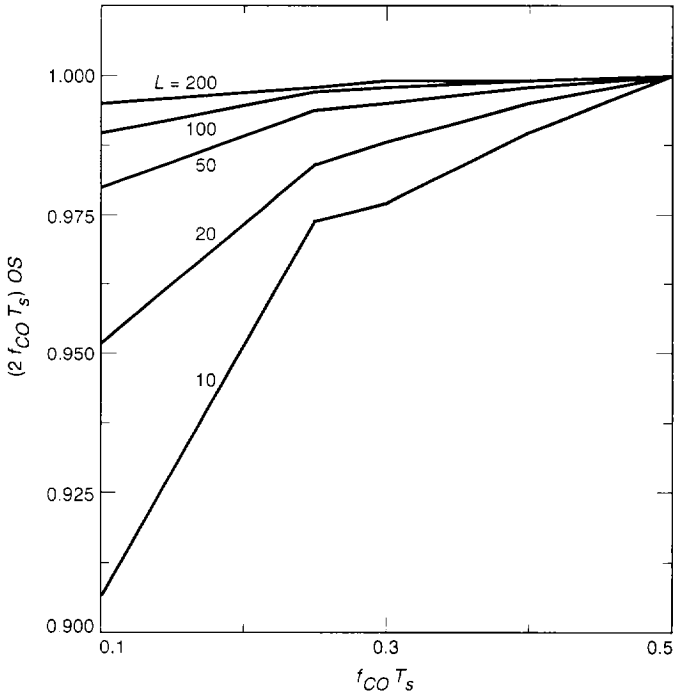


**Fig. 2. Dependence of $(2f_{co}T_s)OS$ versus $f_{co}T_s$ and $L \equiv 5N_{BAUD} - 1$.**

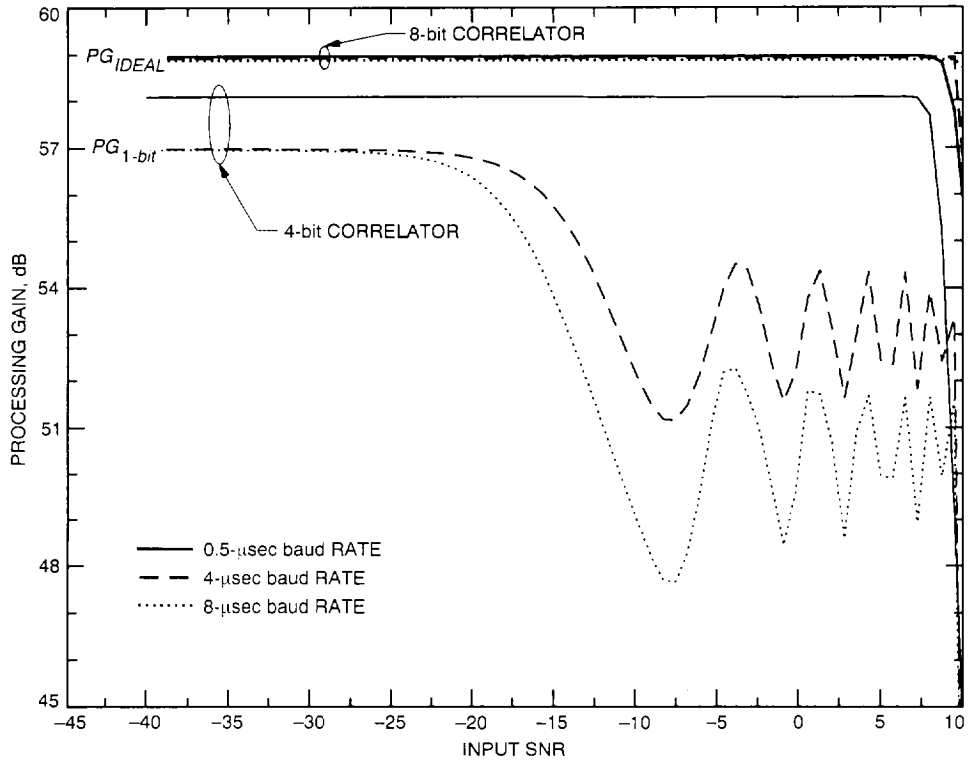


**Fig. 3. Processing gain versus input SNR for 4-bit, 8-bit correlator quantization at constant time–bandwidth product (59 dB).**

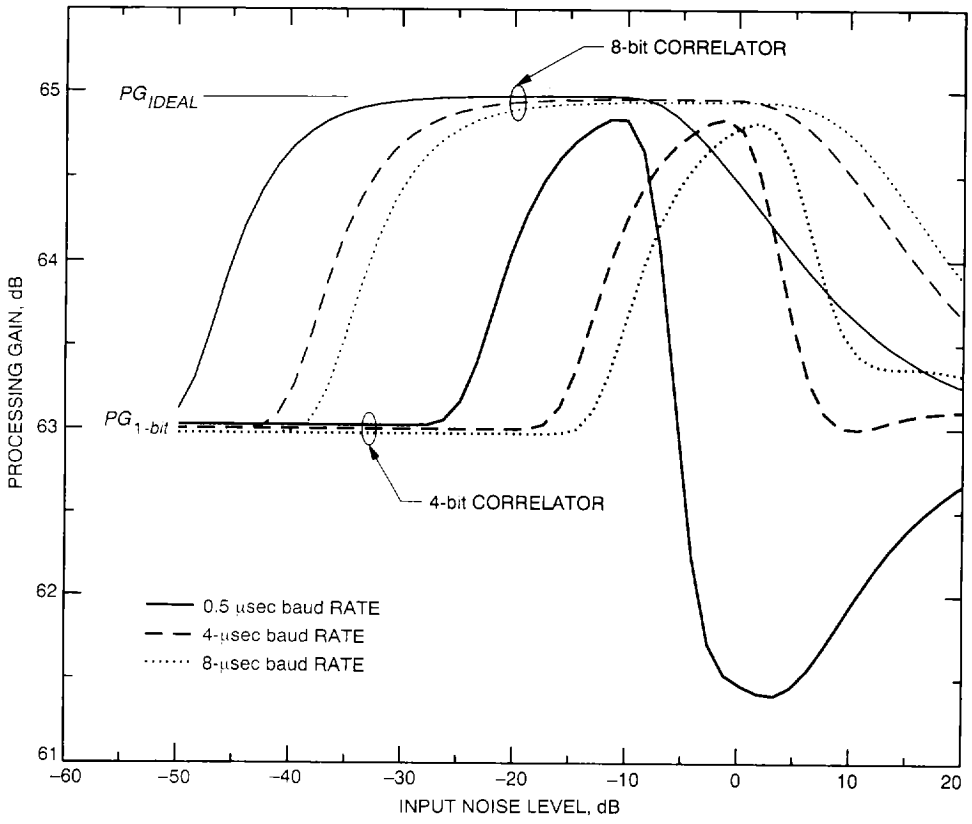


**Fig. 4. Processing gain versus input noise level (decibels referenced to 0.3 × A/D full-scale voltage) at constant SNR (−30 dB) and time–bandwidth product (64.9 dB).**

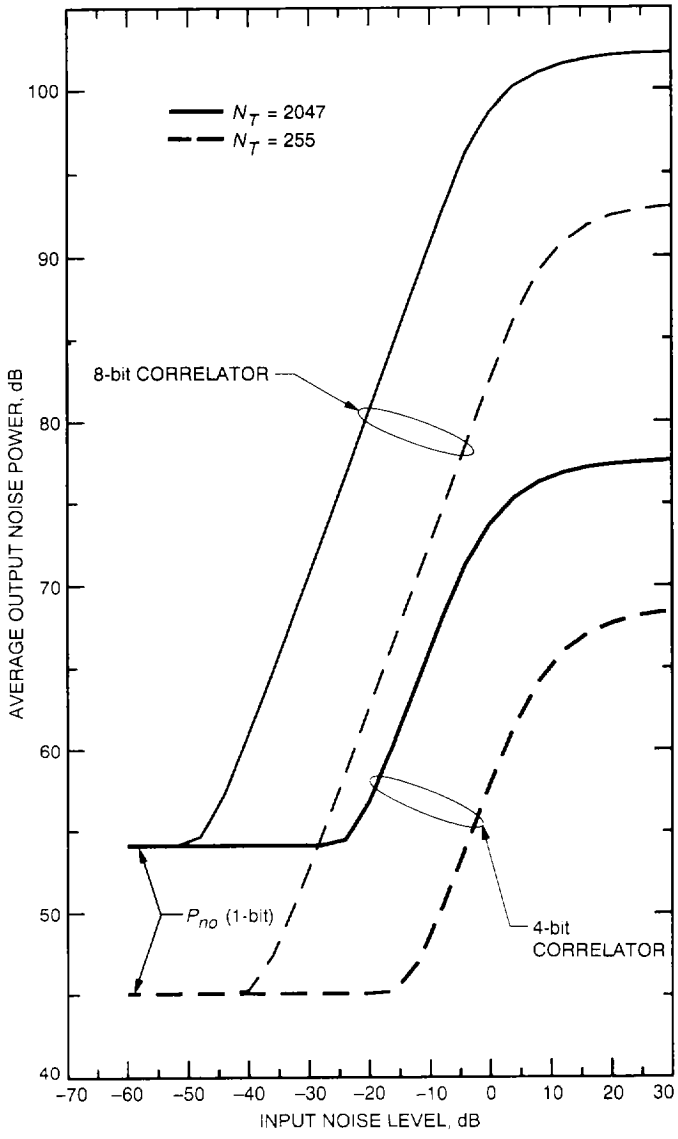


**Fig. 5. Output noise versus input noise level (decibels referenced to 0.3 × A/D full-scale voltage) for 4- and 8-bit correlator quantization.**

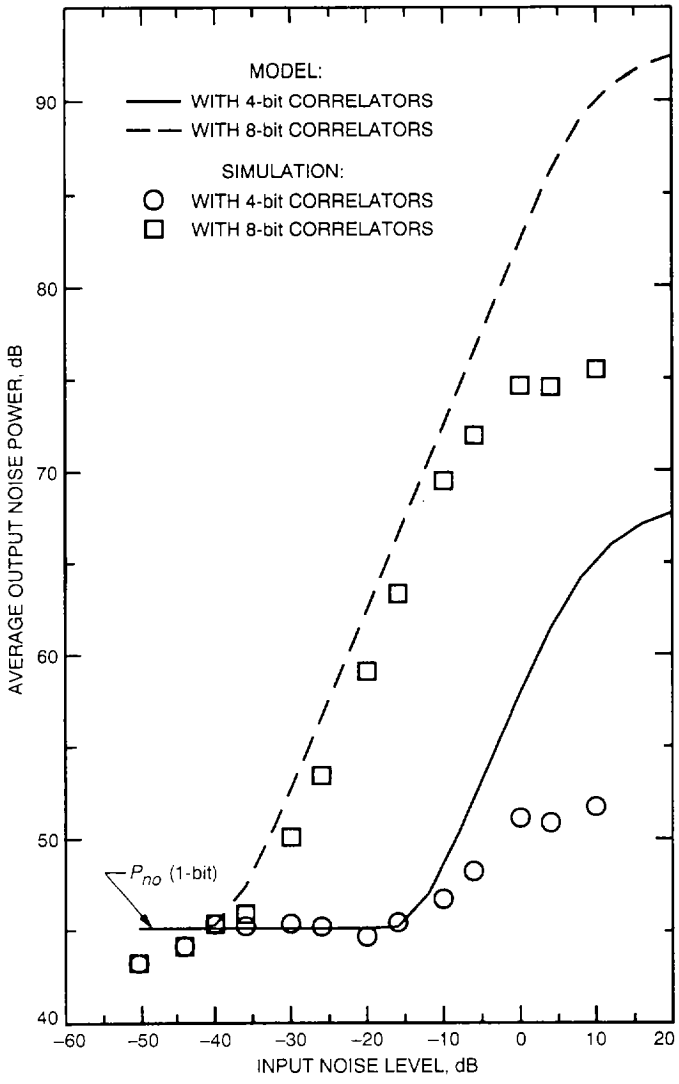


**Fig. 6. Output noise versus input noise level (decibels referenced to 0.3 × A/D full-scale voltage) from statistical model and computer simulation.**